Applied Catalysis B: Environmental 217 (2017) 30–36

Contents lists available at ScienceDirect

Applied Catalysis B: Environmental

journal homepage: www.elsevier.com/locate/apcatb

Self-optimizing bifunctional CdS/Cu_2S with coexistence of light-reduced Cu^0 for highly efficient photocatalytic H_2 generation under visible-light irradiation

Jiajun Zhang, Weisong Li, Ye Li, Lei Zhong, Chunjian Xu*

School of Chemical Engineering and Technology, Chemical Engineering Research Center, State Key Laboratory of Chemical Engineering, Tianjin University, Tianjin 300350, China

ARTICLE INFO

Article history:
Received 2 April 2017
Received in revised form 22 May 2017
Accepted 25 May 2017
Available online 26 May 2017

Keywords:
Self-optimizing
Bifunctional
CdS/Cu_2S
Hydrogen evolution
Photocatalysis

ABSTRACT

A self-optimizing bifunctional core-shell CdS/Cu_2S heterojunction with high activity and superb stability for the photocatalytic hydrogen evolution under visible light irradiation was synthesized by a simple two-step solvothermal method. Compared with pure CdS, the photocatalytic activity of the hybrid is significantly enhanced by almost 25 times. The sample CdS/Cu_2S-30 has shown a maximum H_2 evolution rate of 14.4 mmol h^{-1} g^{-1} with an apparent quantum yield of 19.5% at 420 nm. The surface of single-crystalline CdS nanorod is fully covered by Cu_2S, observed via SEM and TEM, which benefits the activity of catalyst by shorting radial transfer path of charge carriers and increasing the surface area for reaction. This photocatalyst features both bifunction and self-optimizing. During photo reaction, part of Cu_2S is reduced to Cu^0 by irradiation on the surface between CdS core and Cu_2S shell, while the rest of Cu_2S offers plenty of active sites for hydrogen evolution reaction (HER). These generated Cu^0 retard the charge carrier recombination process by forming multi-heterojunction. Meanwhile, the self-optimizing of this photocatalyst is realized by Cu/Cu_2S ratio on the surface of catalyst varying automatically to the optimal value to adapt to the corresponding reaction condition. Based on all these benefits, hydrogen evolution reaction is facilitated.

1. Introduction

Light-driving catalyst-assisted water reducing reaction (LCWR) is considered to be a promising method to tack the global energy and environment crisis [1]. Since Fujushima et al. firstly developed a TiO_2 photocatalyst for hydrogen evolution reaction (HER) from water splitting in 1972 [2], many semiconductor photocatalysts have been studied. Due to the low catalytic activity caused by poor solar spectral responding and high rate recombination of charge carriers in those photocatalysts [3], the practical application of HER is blocked.

Cadmium sulfide (CdS) is a promising semiconductor for HER with a 2.4 eV band gap which matches well with solar spectral [4]. This material was widely studied as a photocatalyst for LCWR [3]. However, the fast recombination of charge carriers consisting of both bulk recombination and surface recombination [5], is the vital factor that results in low catalytic activity and severe photo-corrosion. Different morphologies of CdS nanostructures have been explored to reduce the bulk recombination, such as microspheres, nanopatrticles, nanorods and microsheets [3,5]. The nanorods have been extensively studied because they can benefit the activity of catalyst by shortening radial transfer path of charge carriers and increasing the surface area for reaction [3,5]. Several methods have been developed to reduce the surface recombination, such as cocatalyst loading, heterojunction construction and surface defect modification. Noble metals such as Pt [6], Pd [7], Ru [8], Au [9] et al., have been loaded on CdS as cocatalysts, which was proved to be an effective way. However, its application is limited by the high cost of noble metals. Therefore, nowadays much more attention is focused on exploring non-noble metal and semiconductor as cocatalyst to overcome these drawbacks. Duel cocatalysts, also known as bifunctional cocatalysts, which include one material helping the separation of charge carriers and another offering active sites for HER, have also been applied in photocatalytic HER to enhance its catalytic activity [10].

The potential of Cu_2S conduction band(CB) edge is slightly more negative than the reduction potential of H^+/H_2, making it feasible for HER [11]. Its excellent property in surface reaction of HER

* Corresponding author.
E-mail address: cjxu@tju.edu.cn (C. Xu).

http://dx.doi.org/10.1016/j.apcatb.2017.05.074
0926-3373/

has been noticed and applied to electrocatalytic hydrogen evolution [12]. Meanwhile, under irradiation, Cu^+ in Cu_2S can be easily reduced to Cu^0 [13] which retard the charge carrier recombination process by forming multi-heterojunction [10]. Both excellent characters of Cu_2S make it possible to become an ideal bifunctional cocatalyst in LCWR. Furthermore, the coexistence of Cu_2S and Cu^0 reduced from Cu^+ may exhibit potential function of self-optimizing, which can balance the separation of charge carriers and active sites for HER via varying Cu/Cu_2S ratio on the surface of catalyst.

To the best of our knowledge, there are few papers that have investigated the self-optimizing strategy of photocatalyst in HER [14]. Furthermore, there is no open literature that has reported the application of self-optimizing combined with bifunctional strategy of photocatalyst in HER. In this study, a self-optimizing bifunctional binary core-shell heterostructured CdS/Cu_2S photocatalyst with high activity and superb stability was synthesized for hydrogen evolution via water splitting under visible light. The novel CdS/Cu_2S nanohybrid was synthesized by a simple two-step solvothermal method and characterized to present its crystallography, morphology, spectral features and composition. Furthermore, the bifunctional and self-optimizing features of this material are illustrated for its superiority in catalytic activity and stability.

2. Experimental details

2.1. Chemicals and reagents

All materials are commercial available and used without further purification. Cadmium nitrate tetrahydrate ($Cd(NO_3)_2$, AR, 99%, Sigma-Aldrich Co., Ltd), thiourea (CH_4N_2S, AR, 99%, Sigma-Aldrich Co., Ltd), cuprous chloride(CuCl, AR, 99%, Sigma-Aldrich Co., Ltd), polyvinylpyrrolidone($(C_6H_9NO)_n$, K30, AR, Macklin Co., Ltd), ethylenediamine($C_2H_8N_2$, AR, 99%, Kermal Co., Ltd), ethanol(C_2H_5OH, AR, 99%, Kermal Co., Ltd), glycerol($C_3H_8O_3$, AR, 99%, Kermal Co., Ltd), ethylene glycol($(CH_2OH)_2$, AR, 99%, Kermal Co., Ltd) and distilled water.

2.2. Synthesis

2.2.1. Synthesis of single-crystalline CdS nanorods

Pure CdS nanorods were prepared by a modified one-step solvothermal method [15]. In a typical procedure, 2.28 g of $CdCl_2{\cdot}2.5H_2O$ and 3.02 g of CH_4N_2S were dissolved in 60 mL of ethylenediamine. The mixture was transferred into a Teflon-lined autoclave, sealed, and maintained at 160 °C for 48 h. After cooling to room temperature, the resulting yellow solid products were collected by filtration, washed with distilled water and ethanol several times each. The product was then dried at 80 °C overnight.

2.2.2. Synthesis of CdS/Cu_2S

Cu_2S shells were coated on the surface of CdS nanorods based on the solvothermal reaction. Typically, 0.4 g CdS nanorods and 0.5 g PVP were added into 40 mL glycerol. The mixture was ultrasonicated for 180 min and then stirred at room temperature for 2 h. Then 10 mL aqueous solution of a certain amount of CH_4N_2S was slowly added into the above reaction solution, followed by stirring overnight. Next, 15 mL CuCl ethylene glycol solution (the molar ratio of CH_4N_2S to CuCl was kept at 3) was slowly added to the above solution and then stirred for 5 h. The mixture was transferred into a Teflon-lined autoclave and then maintained at 100 °C for 24 h. Finally, the product was collected by centrifugation and washed with distilled water and ethanol several times each and vacuum-dried overnight to obtain the final powder. The mass ratios of Cu_2S to CdS nanorods were 0, 5%, 10%, 20%, 30%, 40%and 50%, and the corresponding samples were labeled as CdS/Cu_2S-0, CdS/Cu_2S-5, CdS/Cu_2S-10, CdS/Cu_2S-20, CdS/Cu_2S-30, CdS/Cu_2S-40and CdS/Cu_2S-50, respectively. The pure Cu_2S powder sample was prepared following the same procedure without adding CdS nanorods.

2.3. Characterization

Scanning electron microscopy (SEM) was performed on an S-4800(Hitachi, Japan). Transmission electron microscopy (TEM) images, high-resolution transmission electron microscopy (HR-TEM) images were collected on a JEM-2100F (JEOL, Japan) electron microscope, operated at an acceleration voltage of 200 kV. The crystal structures of the samples were investigated by (XRD) powder X-ray diffraction (D8 Advance, Bruker, Germany) using graphite monochromatized Cu Kα radiation of 1.54178 Å, operating at 40 kV and 40 mA. The scanning rate was 5° min^{-1} from 10° to 80° (2θ). The UV–vis absorption spectra were obtained using a UV–vis spectrophotometer (Evolution 300, Thermo Scientific, America). X-ray photoelectron spectroscopy (XPS) measurement was performed using a PHI-5000C ESCA X-ray photoelectron spectrometer (Perkin-Elmer, America).

2.4. Photocatalytic hydrogen production

Photocatalytic H_2 production experiments were carried out in a 120 mL round-bottom flask at ambient temperature. The effective irradiation area of the cell is about 33.18 cm^2.A 300 W Xe-lamp(CEL-HXF300, CEAULIGHT, China) equipped with a 420 nm cut-off filter was used to provide the visible light irradiation. In a typical photocatalytic reaction, 20 mg of the powder sample was dispersed in an 80 mL lactic acid and K_2HPO_4 aqueous solution. Before irradiation, the solution was bubbled with high purity nitrogen for 1 h to remove the air inside. The amount of evolved H_2 was detected online by a gas chromatogram (GC-7890A, Agilent Technologies, America) with a thermal conductivity detector(TCD) and Ar working as carrier gas. The apparent quantum yield (AQY) was measured using a 300 W Xe-lamp (CEL-HXF300, CEAULIGHT, China) equipped with a 420 nm (±5 nm) band pass cut filter. The apparent quantum yield (AQY) was calculated by the Eq. (1).

$$AQY(\%) = \frac{\text{the number of reacted electrons}}{\text{the number of incident photons}} \times 100$$

$$= \frac{\text{the number of evolved } H_2 \text{ molecules} \times 2}{\text{the number of incident photons}} \times 100 \quad (1)$$

3. Results and discussion

The selected samples were investigated by SEM and TEM.

As shown in Fig. 1a, the pure CdS nanorods had a length of 100–200 nm and a diameter of 10–15 nm. Fig. 1b,c demonstrates that after CdS nanorods were coated by Cu_2S, the nanorods remained their original morphology with larger diameter. The shell-core structure and the close integration between these two materials are shown clearly in Fig. 1d. Also, the diameter of CdS nanorod increased by 5–8 nm after deposition of Cu_2S, as shown in Fig. 1c&d and Supplementary data Fig. S1. In the TEM image of coated CdS nanorods(Fig. 1e), a crystal lattice distance of 0.336 nm at the core and 0.281 nm in the shell are demonstrated, which can be indexed to the (002) plane of hexagonal CdS(JCPDS 65-3414) and the (200) plane of Cu_2S(JCPDS 84-1770).

As shown in Fig. 2, the crystalline structure of sample CdS/Cu_2S-10, CdS/Cu_2S-20, CdS/Cu_2S-30, CdS/Cu_2S-40and CdS/Cu_2S-50 were

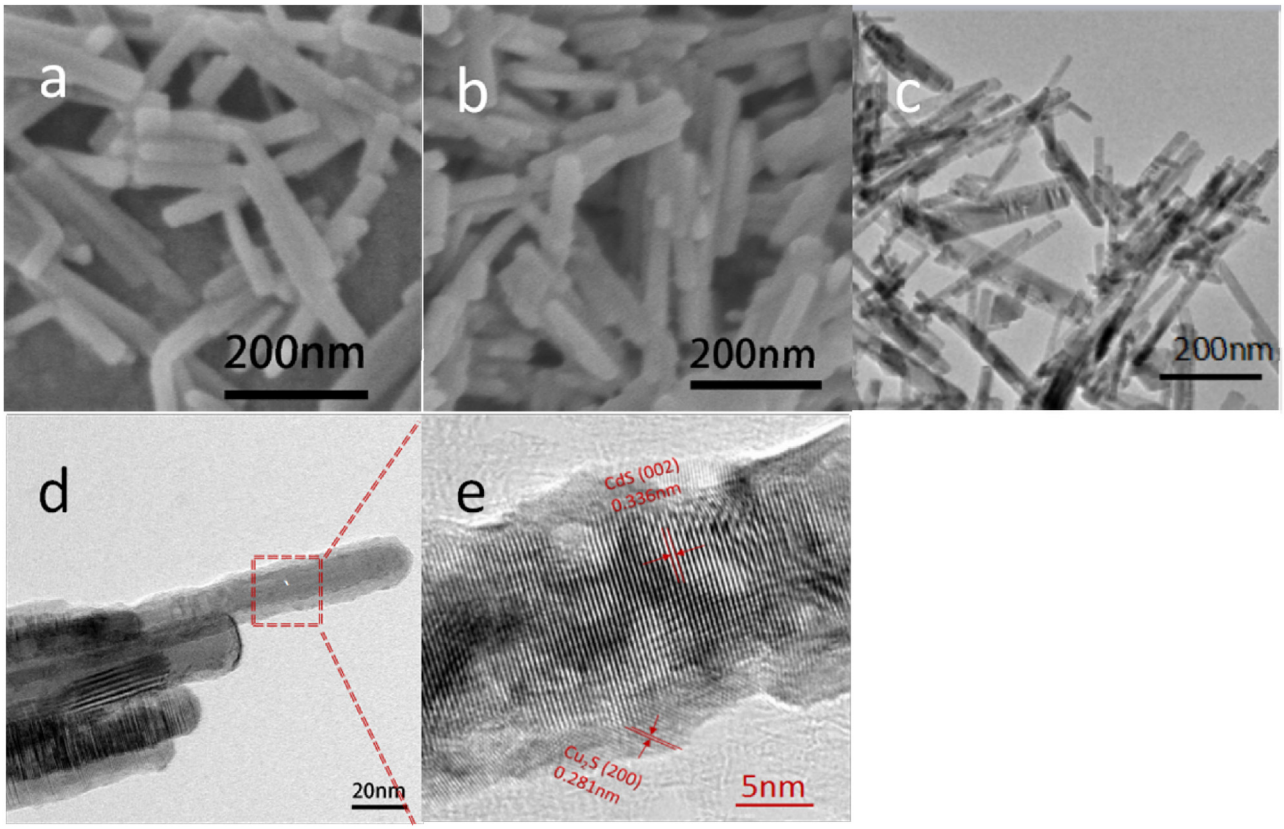

Fig. 1. (a) SEM image of CdS nanorods; (b) SEM image of sample CdS/Cu_2S-10; (c–e)TEM image of CdS/Cu_2S-30.

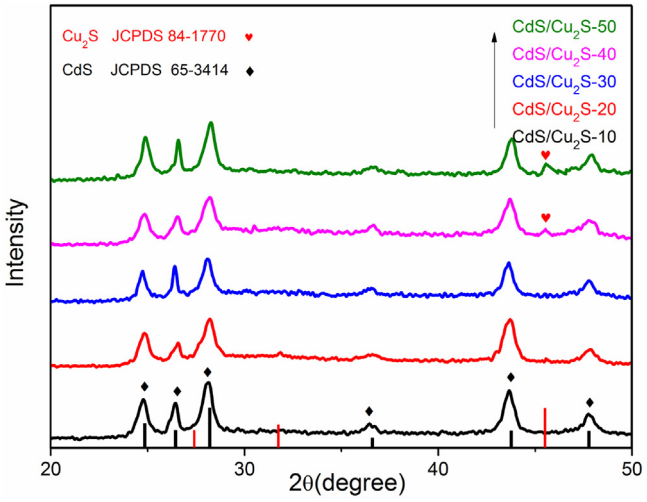

Fig. 2. XRD patterns of CdS/Cu_2S-10, CdS/Cu_2S-20, CdS/Cu_2S-30, CdS/Cu_2S-40, and CdS/Cu_2S-50.

characterized by XRD. All samples can be well-indexed to hexagonal CdS(JCPDS 65-3414). The peak at 24.86°, 26.45°, 28.22°, 36.62°, 43.78° and 47.79° are indexed to diffraction patterns of (100), (002), (101), (102), (110) and (103) lattice planes, respectively. It can be concluded that the pure phase CdS has been successfully synthesized. Although the features of Cu_2S coating on CdS nanorods were clearly observed by TEM(Fig. 1c & Supplementary data Fig. S1), there is no apparent diffraction pattern of Cu_2S in CdS/Cu_2S-10 and CdS/Cu_2S-20, which could be pinned on its low coating. With Cu_2S coating increasing to more than 20 wt%, the peak at 45.55° which is designated to the diffraction pattern from (220) lattice plane of Cu_2S (JCPDS 84-1770) gradually appeared.

The chemical states of elements in catalyst were characterized via X-ray photoeletron spectroscopy(XPS). CdS/Cu_2S-30 was chosen to carry out the XPS measurement. The survey spectrum confirmed the existence of Cd, S, Cu, O and C. The presence of C can be ascribed to the XPS instrument and pump oil residue. The high resolution XPS spectrum in Fig. 3b shows two peaks at 412.6 and 405.8 eV corresponding to the binding energy of Cd^{2+} $3d_{3/2}$ and Cd^{2+} $3d_{5/2}$ in CdS, respectively. Comparing with literature [16], there is a noticeable shift toward higher energy zone which indicates a possible Fermi energy level shift caused by the close interaction [14] between CdS nanorods and Cu_2S coating. In Fig. 3d the peaks at 951.8 and 930 eV which are indexed to the binding energy of Cu^+ $2p_{1/2}$ and Cu^+ $2p_{3/2}$ in Cu_2S shift toward lower energy zone comparing with literature [17] due to the same reason. The two minor peaks at 953.5 and 932.3 eV should be attributed to Cu reduced from Cu_2S in solvothermal reaction. Fig. 3c demonstrates the high resolution XPS spectra of S 2p. The main peak at162.1 eV verifies the existence of CdS, while the minor peak at 160.4 eV is indexed to the binding energy of S^{2-} 2p in Cu_2S. The proportion of the peak areas of these two peaks matches well with the mole ratio of CdS/Cu_2S in this particular sample (Supplementary data Table 1). This result verified the close interaction between two materials and indicated the possibility of a convertible binary/ternary photocatalyst. This theory will be further studied in this work.

The H_2 generation experiment was conducted. Each catalyst was tested for 12 h, and the average rate was demonstrated in Fig. 4. Fig. 4a shows the H_2 evolution rate of each catalyst in lactic acid and K_2HPO_4 mixture solution. Respectively, the corresponding rate of H_2 evolution is 0.58 mmol g^{-1} h^{-1},5.8 mmol g^{-1} h^{-1}, 8.7mmolg^{-1} h^{-1}, 12.1 mmol g^{-1} h^{-1}, 14.4 mmol g^{-1} h^{-1}, 10.0 mmol g^{-1} h^{-1}, 3.2 mmol g^{-1} h^{-1},for pure CdS nanorod,

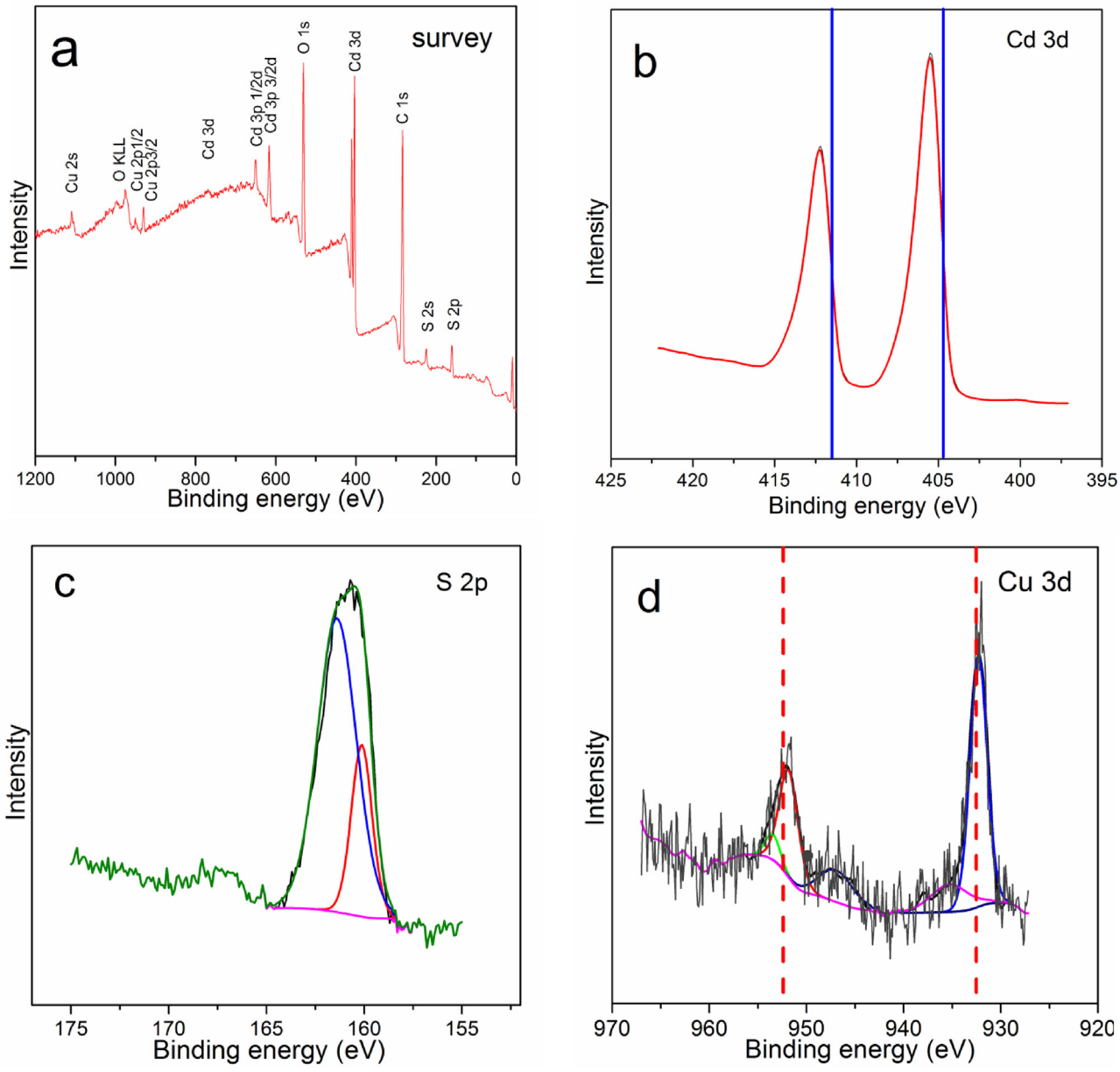

Fig. 3. (a) XPS survey spectrum of sample cu2s/cds-30. High-resolution XPS spectra of (b) Cd 3d, (c)S 2p and (d) Cu 3d in sample cu2s/cds-30.

CdS/Cu_2S-5, CdS/Cu_2S-10, CdS/Cu_2S-20, CdS/Cu_2S-30, CdS/Cu_2S-40 and CdS/Cu_2S-50. The rate of H_2 evolution peaked at CdS/Cu_2S-30 in 14.4 mmol g^{-1} h^{-1}. This CdS/Cu_2S system has a higher rate of H_2 evolution than many other binary and ternary systems without noble metal loading as cocatalyst reported in the previous literature(Supplementary data Table S3). This superiority indicates that Cu_2S loading on nanorod benefits the photo-catalytic activity of CdS.

There is a noticeable decrease in H_2 evolution for the further increase of Cu_2S coating, which was reported as the "shielding effect" [18,19]. The excessive coating will block the sacrificial agent and the light absorption on CdS nanorod partially. As can been seen in Supplementary data Fig. S1, the radius of CdS/Cu_2S-50 nanaorods is evidently larger than that of CdS/Cu_2S-50. Besides, the excessive loading of Cu_2S increases the radius of the charge transporting to the surface of catalyst, thus increases the possibility of charge carrier recombination. This can be well-evidenced by photoluminescence spectra in Fig. 4b. As the photoluminescence is generated from the charge recombination process, weaker luminescence represents less charge carriers recombining [3]. With Cu_2S coating on, the luminescence theatrically decreases, which represents the recombination between photo-generated electrons and holes being retarded. Note that sample CdS/Cu_2S-50 has bigger luminescence than sample CdS/Cu_2S-30 and CdS/Cu_2S-10, implying the increase of charge recombination caused by the excessive loading of Cu_2S. Sample CdS/Cu_2S-30 and CdS/Cu_2S-10 have almost the same luminescence, but different photocatalytic H_2 evolution rates. The reason for this will be discussed later.

The stability of the nanohybrid was obvious. There is no sign of the rate of H_2 evolution dropping in any of 12 h HER test we run. To be further affirmed, a long time stability test was carried out using sample CdS/Cu_2S-30, in lactic acid and 0.25 M K_2HPO_4 solution under visible light for 24 h, and the result is presented in Fig. 4c. The rate of H_2 evolution retains its original speed, suggesting a great stability in Cu_2S/CdS hybrid.

Sample Cu_2S/CdS-30 and pure CdS nanorod were coated on FTO grass working as electrodes to carry out transient photocurrent response curves in a three-electrode electrochemical setup

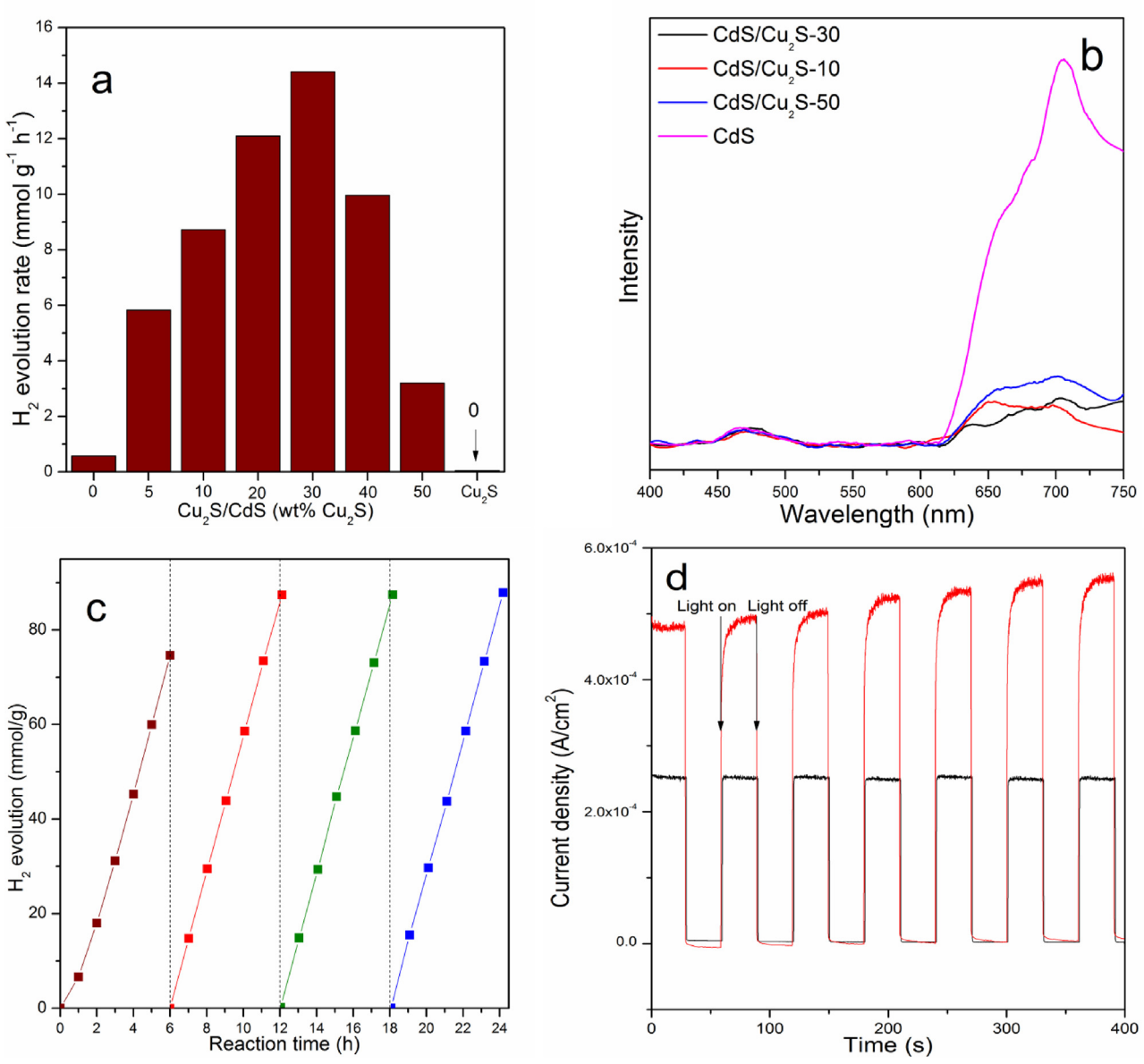

Fig. 4. (a) H_2 evolution rate on the pure CdS nanorod, CdS/Cu_2S-5, CdS/Cu_2S-10, CdS/Cu_2S-20, CdS/Cu_2S-30, CdS/Cu_2S-40 and CdS/Cu_2S-50 using 0.25 M K_2HPO_4 in 10% vol lactic acid solution as sacrificial agent. (b) Cyclic H_2 evolution curve for sample CdS/Cu_2S-30 in 10% vol lactic acid solution. (c) Transient photocurrent responses of the pure CdS nanorod and CdS/Cu_2S-30. (d) photoluminesence spectra of the CdS-a, pure CdS, CdS-a/Cu_2S-30, CdS/Cu_2S-10, CdS/Cu_2S-30, and CdS/Cu_2S-50.

under chopped visible light(> 420 nm). The result presented in Fig. 4d showed that the dark currents of both samples are very low (<10^{-6} A/cm^2), while the photocurrents rapidly increase when the visible light turns on. Specifically, the photocurrent on Cu_2S/CdS-30 electrode is about 3 times higher than that on pure CdS electrode, manifesting that the Cu_2S coating and the close contact between CdS and Cu_2S significantly retard the recombination of photo-generated charge carriers, which would benefit the photocatalytic activity on Cu_2S/CdS-30.

The apparent quantum yield(AQY) test was performed in the optimal sacrificial agent, a 300 w Xe lamp with a 420 nm(±5 nm) band pass filter working as a monochromatic light source. The light intensity of monochromatic light (Supplementary data table S2 & Supplementary data Fig. S2) was measured with a irradiatometer (CEL-NP2000, CEAULIGHT, China). In the first two hours, the AQY of sample CdS/Cu2S-30 is 2.4%. After that, the AQY increased to 19.5%, and remained there (Supplementary data Fig. S3).

Uv-vis absorption spectral of CdS, and CdS/Cu_2S-30 were presented in Supplementary data Fig. S5. As a wide band gap semiconductor, CdS can absorb light up to 560 nm(2.2 ev) [3,5]. With Cu_2S coating on the surface, CdS nanorod become a better absorber of light, owing to the narrower band gap of Cu_2S. The color of catalyst changed from brilliant yellow to dark green with Cu_2S coating on the surface, which also implied the enhancement in light absorption.

As we predicted, the rate of H_2 evolution was much lower at the beginning of irradiation than that in the subsequent process (Supplementary data Fig. S4). The experimental phenomena were illustrated based on HER test and XPS measurement. Due to the poor locomotivity of charge carriers in Cu_2S, the photo-generated electrons translated from CB of CdS stagnate at surface between CdS core and Cu_2S shell. These surplus electrons have enough energy to reduce Cu^1 in Cu_2S into Cu^0 [13]. The Cu/Cu_2S ratio on the surface of catalyst is able to be optimized automatically depending on two factors. Too much Cu will lead to lesser active sites of HER, while

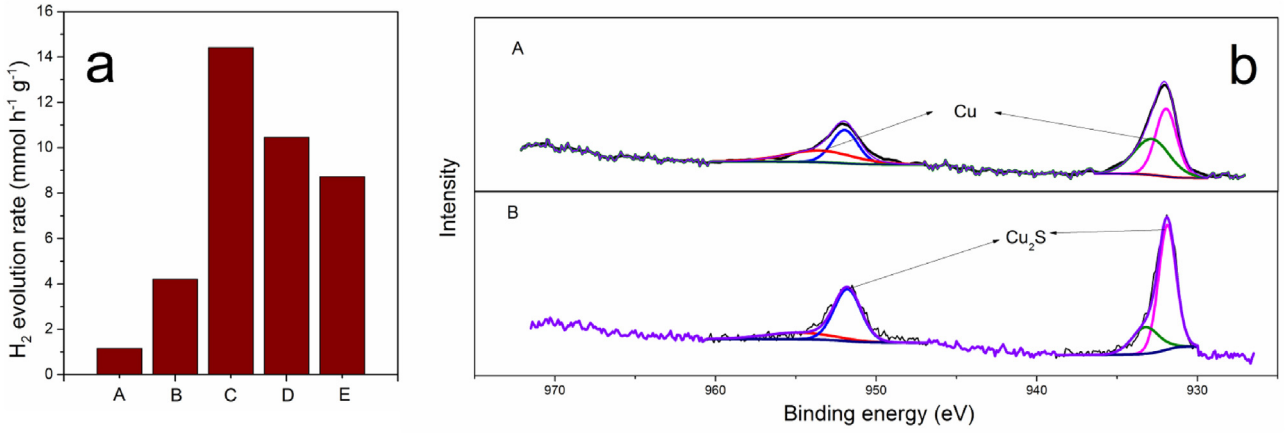

Fig. 5. (a) The rate of H_2 production using sample CdS/Cu_2S-30 under different sacrificial solution: (A) 0.35 M Na_2S + 0.25 M Na_2SO_3, (B) 10% vol lactic acid solution, (C) 0.25 M K_2HPO_4 in 10% vol lactic acid solution, (D) 0.35 M K_2HPO_4 in 10% vol lactic acid solution, (E) 0.5 M K_2HPO_4 in 10% vol lactic acid solution. (b) High resolution XPS spectra of Cu 2p in sample CdS/Cu_2S-30 using (A) 10% vol lactic acid solution, (B) 0.35 M K_2HPO_4 in 10% vol lactic acid solution as sacrificial agent after irradiation.

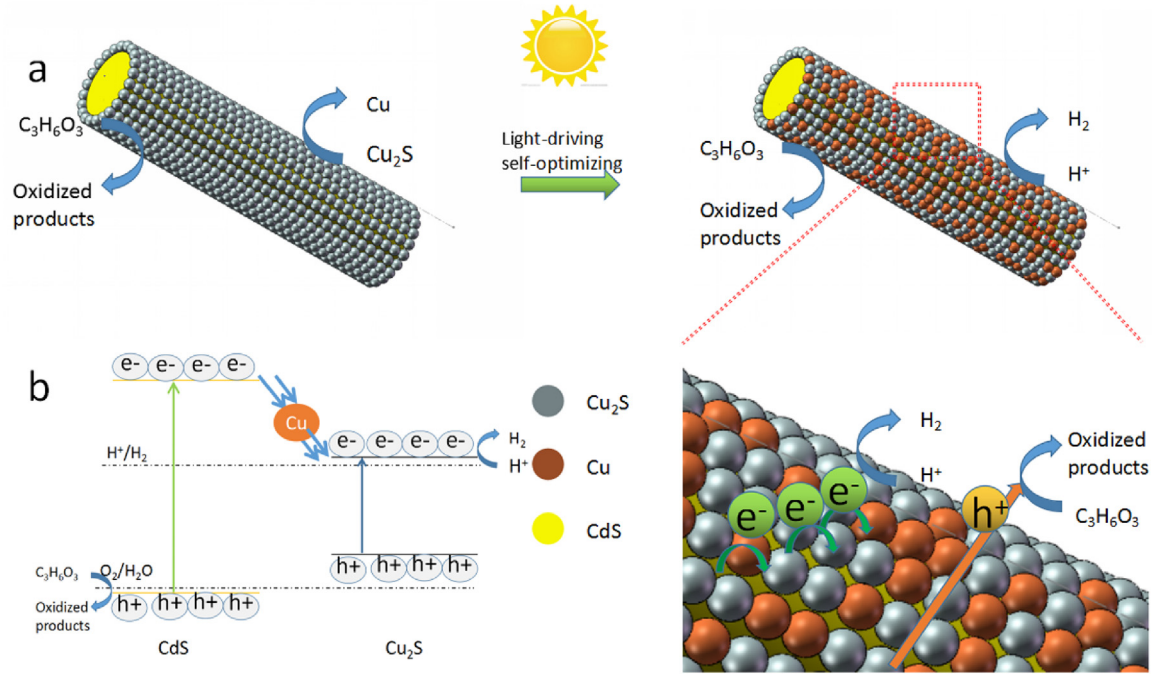

Fig. 6. (a)Schematic illustration of light-driving self-optimizing process on CdS/Cu_2S core-shell hybrid. (b) Schematic illustration of photocatalytic HER process on Cu@CdS/Cu_2S core-shell hybrid.

lesser Cu will lead to bigger chance of the recombination between photo-generated electrons and holes. Both factors will retard the light-reduction process. Besides, as the VB top of CdS is 1.25 V(vs NHE) [6] and the electrode potential of Cu^+/Cu is 0.52 V(vs NHE) [14], the light-reduction Cu^0 can be oxidized to Cu^+ by the powerful photo-generated holes at the VB of CdS and then recrystallizes as Cu_2S in situ. The amount of the Cu_2S active sites which are needed for higher reaction rate varies automatically to the optimal value to adapt to the corresponding hydrogen ion concentration in the solution. By introducing a certain amount of K_2HPO_4 into the sacrificial solution, we can control the pH value of solution, which determines the Cu/Cu_2S ratio on the surface of catalyst. Note that lower pH value favors more Cu^1 reduced into Cu^0. The CdS/Cu_2Sbinary system will start to transform to a Cu@CdS/Cu_2Sternary system when the reaction begins until the dynamic equilibrium of the transform between Cu^0 and Cu_2S is reached.

A validation experiment was designed based on above analysis. In Fig. 5a, the catalytic activity of the same catalyst CdS/Cu_2S-30 varied with the different amount of K_2HPO_4 in 10% vol lactic acid solution. The sample was irradiated in 10% vol lactic acid solution and in 10% vol lactic acid solution with 0.5 M K_2HPO_4, then marked as sample A and sample B, respectively. The used catalyst was collected by filtration after irradiation, washed with water repeatedly and dried at 40 °C. These two samples were analyzed by XPS to investigate if there was any transformation in chemical state. There was a significant change in the Cu^+ $2p_{1/2}$ and Cu^+ $2p_{3/2}$ spectrum, not only before and after irradiation, but also between different compositions of sacrificial solution. Comparing sample Cu_2S/CdS-30, A and B, the Cu/Cu_2S ratio shown a noticeable difference corresponding to different reaction condition. It can be seen in Fig. 5b and Supplementary data Table 1, that Cu^0 generated from light-reduction of Cu_2S, and the Cu/Cu_2S ratio got lower while the pH value of sacrificial solution went higher. These results confirm

our prediction about a convertible binary/ternary photocatalyst with self-optimizing capacity to adapt to changed circumstances. The surface recombination of charge carriers is replaced by the dynamic equilibrium of the transform between Cu^0 and Cu_2S, thus the photo-corrosion is blocked and the excellence stability of this CdS based photocatalyst can be achieved.

According to above results, the proposed mechanism for H_2 evolution assisted by Cu_2S/CdS is illustrated in Fig. 6. Under irradiation, electron-hole pairs are generated in CdS core. The more portable electrons at the core CdS 'drop' to the CB of Cu_2S, for CdS is a n-type semiconductor [3]. At the beginning of irradiation, some of photo-generated electrons participate in H_2 generation, while the rest of electrons reduce Cu_2S into Cu^0 partially (Fig. 6a). The self-optimizing of the catalyst proceeds till the Cu^0/Cu_2S ratio varies automatically to the optimal value. Cu_2S acting as active sites for HER, while the light-reduced Cu^0 accelerate the separation process of photo-generated electrons and holes by forming heterojunction [13]. And the separated holes staying at the VB of CdS core are scavenged by the lactic acid simultaneously (Fig. 6b).

4. Conclusions

In this work, a self-optimizing bifunctional core-shell CdS/Cu_2S heterojunction with high activity and superb stability for hydrogen evolution via water splitting under visible light was firstly synthesized by a simple two-step solvothermal method. The photocatalytic activity of the hybrid significantly was increased by almost 25 times compared with pure CdS, with the maximum H_2 evolution rate of 14.4 mmol h^{-1} g^{-1} and an apparent quantum yield of 19.5% at 420 nm under optimal conditions. The application of self-optimizing bifunctional mechanism might become a promising strategy for designing superior photocatalyst in clean energy production.

Acknowledgment

The authors would like to thank Dr. Zhen Li for his help to this work.

Appendix A. Supplementary data

Supplementary data associated with this article can be found, in the online version, at http://dx.doi.org/10.1016/j.apcatb.2017.05.074.

References

[1] J. Liu, Y. Liu, N. Liu, Y. Lifshitz, S. Lee, J. Zhong, Science 347 (2015) 967–970.
[2] A. Fujishima, K. Honda, Nature (1972) 37–38.
[3] D. Sudha, P. Sivakumar, Chem. Eng. Prog. 97 (2015) 112–133.
[4] K. Wu, Y. Du, H. Tang, Z. Chen, T. Lian, J. Am. Chem. Soc. 137 (2015) 10224–10230.
[5] F. Vaquero, R.M. Navarro, J.L.G. Fierro, Appl. Catal. B: Environ. 203 (2017) 753–767.
[6] W. Li, J.R. Lee, F. Jäckel, ACS Appl. Mater. Inter (2016) 29434–29441.
[7] H. Yan, J. Yang, G. Ma, G. Wu, X. Zong, Z. Lei, J. Shi, C. Li, J. Catal. 266 (2009) 165–168.
[8] E. Nosheen, S.M. Shah, Z. Iqbal, J. Photochem. Photobiol. B 167 (2017) 117–127.
[9] L. Wang, R. Li, J. Liu, J. Han, M. Huang, J. Mater. Sci. 52 (2017) 1847–1855.
[10] J. He, D.W. Shao, L.C. Zheng, L.J. Zheng, D.Q. Feng, J.P. Xu, X.H. Zhang, W.C. Wang, W.H. Wang, F. Lu, H. Dong, Y.H. Cheng, H. Liu, R.K. Zheng, Appl. Catal. B: Environ. 203 (2017) 917–926.
[11] J. Zhang, J. Yu, Y. Zhang, Q. Li, J.R. Gong, Nano. Lett. 11 (2011) 4774–4779.
[12] M. Fan, R. Gao, Y. Zou, D. Wang, N. Bai, G. Li, X. Zou, Electrochim. Acta 215 (2016) 366–373.
[13] P.S. Kumar, S. Lakshmi Prabavathi, P. Indurani, S. Karuthapandian, V. Muthuraj, Sep. Purif. Technol. 172 (2017) 192–201.
[14] Z. Zhang, K. Liu, Y. Bao, B. Dong, Appl. Catal. B: Environ. 203 (2017) 599–606.
[15] S. Cao, C. Wang, X. Lv, Y. Chen, W. Fu, Appl. Catal. B: Environ. 162 (2015) 381–391.
[16] O. Tkachenko, E. Shpiro, M. Wark, G. Schulz-Eklof, N. Jaeger, J. Chem. Soc. Faraday Trans. 21 (1993) 3987–3994.
[17] D.L. Perry, A. Taylor, J. Mater. Sci. Lett. 4 (1986) 384–386.
[18] J. Yu, T. Ma, S. Liu, Phys. Chem. Chem. Phys. 13 (2011) 3491–3501.
[19] Q. Li, B. Guo, J. Yu, J. Ran, B. Zhang, H. Yan, J.R. Gong, J. Am. Chem. Soc. 133 (2011) 10878–10884.